Hic-5 expression is a major indicator of cancer cell morphology, migration, and plasticity in three-dimensional matrices

Anushree C. Gulvady, Fatemeh Dubois, Nicholas O. Deakin, Gregory J. Goreczny, and Christopher E. Turner*
Department of Cell and Developmental Biology, State University of New York Upstate Medical University, Syracuse, NY 13210

ABSTRACT **The focal adhesion proteins Hic-5 and paxillin have been previously identified as key regulators of MDA-MB-231 breast cancer cell migration and morphologic mesenchymal-amoeboid plasticity in three-dimensional (3D) extracellular matrices (ECMs). However, their respective roles in other cancer cell types have not been evaluated. Herein, utilizing 3D cell–derived matrices and fibronectin-coated one-dimensional substrates, we show that across a variety of cancer cell lines, the level of Hic-5 expression serves as the major indicator of the cells primary morphology, plasticity, and in vitro invasiveness. Domain mapping studies reveal sites critical to the functions of both Hic-5 and paxillin in regulating phenotype, while ectopic expression of Hic-5 in cell lines with low endogenous levels of the protein is sufficient to induce a Rac1-dependent mesenchymal phenotype and, in turn, increase amoeboid-mesenchymal plasticity and invasion. We show that the activity of vinculin, when coupled to the expression of Hic-5 is required for the mesenchymal morphology in the 3D ECM. Taken together, our results identify Hic-5 as a critical modulator of tumor cell phenotype that could be utilized in predicting tumor cell migratory and invasive behavior in vivo.**

Monitoring Editor
Diane Barber
University of California, San Francisco

Received: Feb 6, 2018
Revised: Apr 3, 2018
Accepted: May 8, 2018

INTRODUCTION

Individual cancer cells can utilize two distinct and sometimes interconvertible modes of motility to migrate through diverse three-dimensional (3D) microenvironments for efficient invasion into the tumor stroma and circulatory system (Sahai and Marshall, 2003; Wolf and Friedl, 2006; Sanz-Moreno *et al.*, 2008; Deakin and Turner, 2011; Friedl and Alexander, 2011). Cells exhibiting an amoeboid mode of migration have a rounded morphology, lack or have limited cell–matrix adhesions and require Rho/ROCK-dependent actomyosin contractility, to promote the formation of membrane blebs, and thereby allowing cells to spatially navigate through voids in the extracellular matrix (ECM; Sahai and Marshall, 2003). On the other hand, cells exhibiting the mesenchymal mode of migration exhibit an elongated morphology, and generate Rac1-dependent protrusions and robust integrin-mediated cell–matrix adhesions that allow these cells to translocate along parallel arrays of ECM bundles (Sanz-Moreno *et al.*, 2008). Additionally, mesenchymal cell migration is associated with matrix metalloproteinase (MMP)-driven matrix remodeling (Sanz-Moreno *et al.*, 2008). Spontaneous interconversion between these two modes of migration termed "plasticity," allows certain tumor cell populations to adapt to local changes in the stromal ECM. Indeed, the matrix architecture in the microenvironment plays an important role in governing the 3D morphology of cancer cells, with loose and soft microenvironments favoring amoeboid-mediated migration, while stiffer and dense matrices favor mesenchymal morphologies (Friedl and Wolf, 2010) which have also been linked to increased tumor malignancy in vivo (Boyd *et al.*, 2011). Additionally, phenotypic plasticity is thought to be one of the primary ways by which more aggressive tumor cell types can evade MMP-targeted therapeutic interventions (Friedl and Wolf, 2003).

Several studies have reported the presence of amoeboid-like cells isolated from different human malignancies including

This article was published online ahead of print in MBoC in Press (http://www.molbiolcell.org/cgi/doi/10.1091/mbc.E18-02-0092) on May 17, 2018.

The authors declare no competing interests.

*Address correspondence to: Christopher E. Turner (turnerce@upstate.edu).

Abbreviations used: 1D, one-dimensional; 2D, two-dimensional; 3D, three-dimensional; ANOVA, analysis of variance; BSA, bovine serum albumen; CAFs, cancer associated fibroblasts; DAPI, 4′6-diamidine-2″-phenylindole; ECM, extracellular matrix; MMP, matrix metalloproteinase; PBST, phosphate-buffered saline/Tween 20; PLA, proximity ligation assay; WT, wild type.

lymphomas, leukemia, breast carcinomas, small-cell lung carcinomas, prostate carcinoma, metastatic sarcomas, and melanomas (Sjogren *et al.*, 1977; Sjogren and Garwicz, 1980; Rintoul and Sethi, 2002; Condeelis and Segall, 2003; Wolf *et al.*, 2003b; Belletti *et al.*, 2008; Gadea *et al.*, 2008; Sanz-Moreno *et al.*, 2008; Sanz-Moreno and Marshall, 2009). Similarly, there is evidence for individual mesenchymal cancer cells obtained from fibrosarcomas, glioblastomas, and melanomas (Friedl and Wolf, 2003; Sanz-Moreno and Marshall, 2009). A number of signaling proteins, for example, FilGAP, DOCK3, ARHGAP22, and GEF-H1, that impact the Rho family of GTPase activity have been identified as being important in the regulation of amoeboid and mesenchymal cancer cell morphology (Sanz-Moreno *et al.*, 2008; Eitaki *et al.*, 2012; Nishi *et al.*, 2015). Nevertheless, from diagnostic and a targeted therapy standpoint, it would be beneficial if the expression level of a specific protein(s) could be used as a predictor of cancer cell phenotype and their respective capacity to exhibit phenotypic plasticity.

Our previous work, using the MDA-MB-231 breast cancer cell line has implicated the closely related focal adhesion proteins, Hic-5 and paxillin, as critical determinants of tumor cell morphology and plasticity (Deakin and Turner, 2011). At focal adhesions, Hic-5 and paxillin are molecular scaffolds that respond to the changes in integrin-ECM signaling by coordinating protein–protein interactions, ultimately leading to the remodeling of the cytoskeleton and facilitating cell migration (Deakin *et al.*, 2012b). Experimental manipulation of Hic-5 and paxillin levels using RNA interference (RNAi) or overexpression in the highly plastic MDA-MB-231 cells was shown to reciprocally influence the amoeboid and mesenchymal phenotypes, as well as the plasticity of these cells in 3D ECM and to inhibit their metastatic potential in vivo (Deakin and Turner, 2011). In addition, Hic-5 is upregulated during TGF-β–induced epithelial to mesenchymal transition to promote invasion (Pignatelli *et al.*, 2012), a process that is arguably also associated with increased tumor malignancy (Yeung and Yang, 2017), suggesting that Hic-5 expression may serve as a prognostic indicator of tumor cell invasion strategies.

Herein, a comparison of the Hic-5 and paxilllin expression levels in various cancer cell lines revealed a striking correlation and causal relationship between the level of Hic-5 protein and 3D cancer cell morphology, plasticity, and invasiveness. By performing domain mapping of Hic-5 and paxillin, we identify key sites within Hic-5 and paxillin that are responsible for promoting distinct mesenchymal and amoeboid morphologies and we identify a critical role for vinculin activity in conjunction with Hic-5 expression in driving cells toward a mesenchymal mode of migration. Our data highlight the importance of Hic-5 expression as a key determinant of cancer cell invasive phenotype and plasticity and furthermore identifies Hic-5 as a prospective marker of tumor migration and invasion behavior that could potentially be used to formulate optimal treatment strategies.

RESULTS

Expression of Hic-5 correlates with cancer cell morphology in 3D ECM invasiveness and phenotypic plasticity

MDA-MB-231 breast cancer cells typically exhibit both mesenchymal and amoeboid migratory phenotypes in 3D ECM and readily undergo switching between these two modes of migration. Our previous studies demonstrated that experimental manipulation of Hic-5 and paxillin levels in MDA-MB-231 breast cancer cells through RNAi or ectopic overexpression, reciprocally impacted cell morphology and attenuated invasion in 3D matrices (Deakin and Turner, 2011). Interestingly, upon screening of a variety of additional cancer cell lines including melanoma (A375P), pancreatic cancer (AsPC-1, MIA-PaCa-2, and BxPC-3), fibrosarcoma (HT1080), and breast cancer (MDA-MB-231) cells, we found widely varying (greater than 10-fold) expression levels of Hic-5 (Figure 1, A and B), while the levels of paxillin were more comparable in all lines tested (a less than twofold change; Figure 1, A and C), resulting in a broad range of Hic-5:paxillin expression ratios (Figure 1D). When plated on two-dimensional (2D) fibronectin-coated glass coverslips, all of the cell lines spread well and formed robust focal adhesions that occupied a comparable area per cell (Figure 1, E and F), indicating functional integrin-mediated cell adhesion. Strikingly, however, when seeded into fibronectin-rich 3D cell-derived matrices (3D CDMs), the individual cell lines exhibited distinct morphologies that correlated closely with the relative expression level of Hic-5 (Figure 1G). For example, cell lines that expressed low levels of endogenous Hic-5 (AsPC-1 and A375P) exhibited an ellipsoid or amoeboid morphology, while those with the highest levels of Hic-5 (HT1080 and MDA-MB-231) exhibited a predominantly elongated or mesenchymal morphology, interspersed with rounded or amoeboid cells resulting in a high average relative morphology index (Figure 1, G and H).

We further investigated the migration rates of these cell lines on 3D CDMs and found that the low Hic-5–expressing cells (AsPC-1, A375P, and MIA-PaCa-2) had slow, but measurable migration velocities (Figure 2, A and B), comparable to previous reports (Sanz-Moreno *et al.*, 2008), while the high Hic-5–expressing cells migrated the fastest (Figure 2, A and B). Additionally, directional persistence followed a similar, but less robust trend in relation to Hic-5 expression (Figure 2C). The invasiveness of the cell lines, as measured by the capacity to migrate through dense 3D collagen–fibronectin plugs (Caswell *et al.*, 2007; Provenzano *et al.*, 2008; Rowe *et al.*, 2009) also correlated positively with the relative Hic-5 to paxillin ratio, with cells having the highest Hic-5:paxillin ratios exhibiting the greatest invasive capacities (Figure 2D). Furthermore, cell lines with the highest levels of Hic-5 exhibited a greater ability to spontaneously switch between the amoeboid and mesenchymal morphologies (Figure 3, A and B). For example, real-time imaging of AsPC-1 cells, which have the lowest Hic-5:paxillin ratio, revealed a very limited ability (<10%) to transition between phenotypes, with most cells remaining amoeboid throughout the assay. In contrast, HT1080 and MDA-MB-231 cells, which have the highest Hic-5:paxillin ratios, were more plastic, with the majority of cells (50–75%, respectively) transitioning frequently between the two phenotypes (Figure 3, A and B). The connection between the relative Hic-5:paxillin expression ratio and cell plasticity is further supported by Pearson's correlation analysis (Figure 3C).

Together, these data indicate that the endogenous level of Hic-5 protein, combined with the Hic-5:paxillin ratio is a robust predictor of cancer cell morphology, phenotypic plasticity, and invasiveness in 3D matrices in a variety of cancer cell types including melanoma, pancreatic, fibrosarcoma, and breast cancer, while the same cell lines all exhibit similar morphologies on 2D substrates. Interestingly, we were unable to identify any cancer cell lines that lacked, or expressed very low levels of paxillin, suggesting that although it is not as robust an indicator of cell phenotype as Hic-5, paxillin nevertheless plays an essential role, in concert with Hic-5 in controlling 3D cancer morphology, migration, and plasticity as previously reported (Deakin and Turner, 2011).

Hic-5 and paxillin inversely regulate morphology and one-dimensional migration on micropatterned substrates

The morphology and migration of cells on narrow micropatterned lines of fibronectin, described as one-dimensional (1D) migration, has been shown to resemble that of cells migrating in 3D ECM both

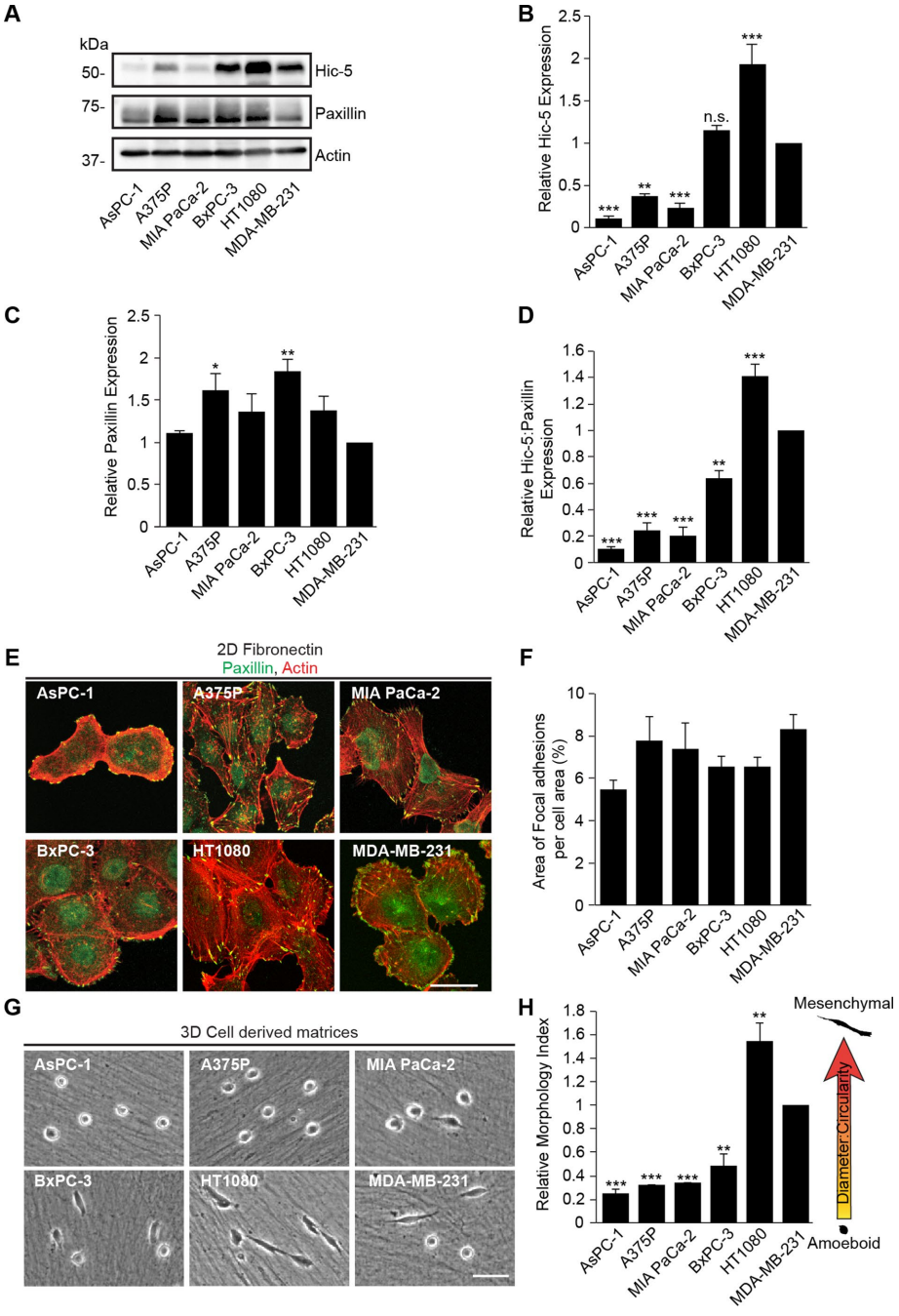

FIGURE 1: The expression of Hic-5 correlates with cancer cell morphology in 3D matrices. (A) Representative Western blot of the expression of Hic-5 and paxillin across various cancer cell lines. Quantitation of the relative expression of (B) Hic-5, (C) paxillin, and (D) Hic-5:paxillin ratio across the cancer lines. (E) Immunofluorescence images of the cancer cell lines plated on 2D fibronectin-coated glass coverslips. (F) Quantitation of the percent of cell area occupied by focal adhesions (n = at least 20 cells). Scale bar = 25 μm. (G) Phase contrast images of the cancer cell lines plated into 3D cell–derived matrices (CDMs). Scale bar = 50 μm. (H) Quantitation of the relative morphology index of the cancer cell lines relative to MDA-MB-231 cells (n = at least 40 cells). Data represent mean ± SEM of at least three independent experiments. One-way ANOVA using Dunnet's multiple comparison test was performed. *, $p < 0.05$; **, $p < 0.01$; and ***, $p < 0.001$.

in vitro and in vivo (Doyle *et al.*, 2009; Tseng *et al.*, 2011). When we plated the various cancer cells documented in Figure 1 on fibronectin-coated micropatterned lines, cell lines with the lowest levels of Hic-5 (AsPC-1 and A375P) were unable to spread effectively and had shorter cell lengths, while those with a higher Hic-5:paxillin ratio (HT1080 and MDA-MB-231) spread linearly along the narrow micropatterned lines (Figure 4, A and B), consistent with their primary morphology when plated into 3D CDMs (Figure 1G). Furthermore, RNAi knockdown of Hic-5 in MDA-MB-231 cells (Figure 4, C and D) caused them to exhibit significantly shorter cell lengths on the micropatterned lines as compared with control RNAi-treated cells (Figure 4, E and F). Conversely, knockdown of paxillin (Figure 4, C and D) resulted in the cells becoming more elongated as compared with the control cells (Figure 4, E and F), consistent with our previous results in 3D CDMs (Deakin and Turner, 2011). Time-lapse imaging over 8 h indicated that although the control cells migrated unidirectionally on the lines of fibronectin, knockdown of either Hic-5 or paxillin reduced migration velocity (Figure 4, G and H). Cells depleted of paxillin became "hypermesenchymal," as previously described in 3D CDMs (Deakin and Turner, 2011), and had lower migration velocities. In contrast, cells with a knockdown of Hic-5 exhibited a unidirectional migration with lower migration velocities than controls (Figure 4, G and H). Conversely, MDA-MB-231 cells overexpressing GFP-paxillin had shorter cell lengths and reduced adhesions, whereas those overexpressing GFP-Hic-5 were more elongated on the lines and formed GFP-Hic-5–positive adhesions (Figure 4, I–K). These data indicate that Hic-5 and paxillin protein levels regulate cell morphology and 1D migration in a similar way to that observed in 3D ECMs and thus the micropatterned lines represent a useful, well-defined model system to further explore signaling mechanisms associated with 3D tumor cell migration.

Distinct LD domains and phosphorylation sites within Hic-5 and paxillin influence 3D morphologies

Hic-5 and paxillin share extensive homology, with both containing multiple N-terminal LD motifs and C-terminal LIM domains (Figure 5, A and F; Thomas *et al.*, 1999; Tumbarello *et al.*, 2002; Brown and Turner, 2004). These motifs interact with a variety of shared and distinct proteins to coordinate the remodeling of the cytoskeleton and regulate cell migration (Brown and Turner, 2004; Deakin and Turner, 2008). Hic-5 and paxillin also contain tyrosine phosphorylation sites Y38/60 and Y31/118, respectively, that are critical to their function by serving as binding sites for SH2-containing adapter and signaling proteins (Burridge *et al.*, 1992; Bellis *et al.*, 1995; Hetey *et al.*, 2005; Zaidel-Bar *et al.*, 2007; Pignatelli *et al.*, 2012). To determine the sites within Hic-5 responsible

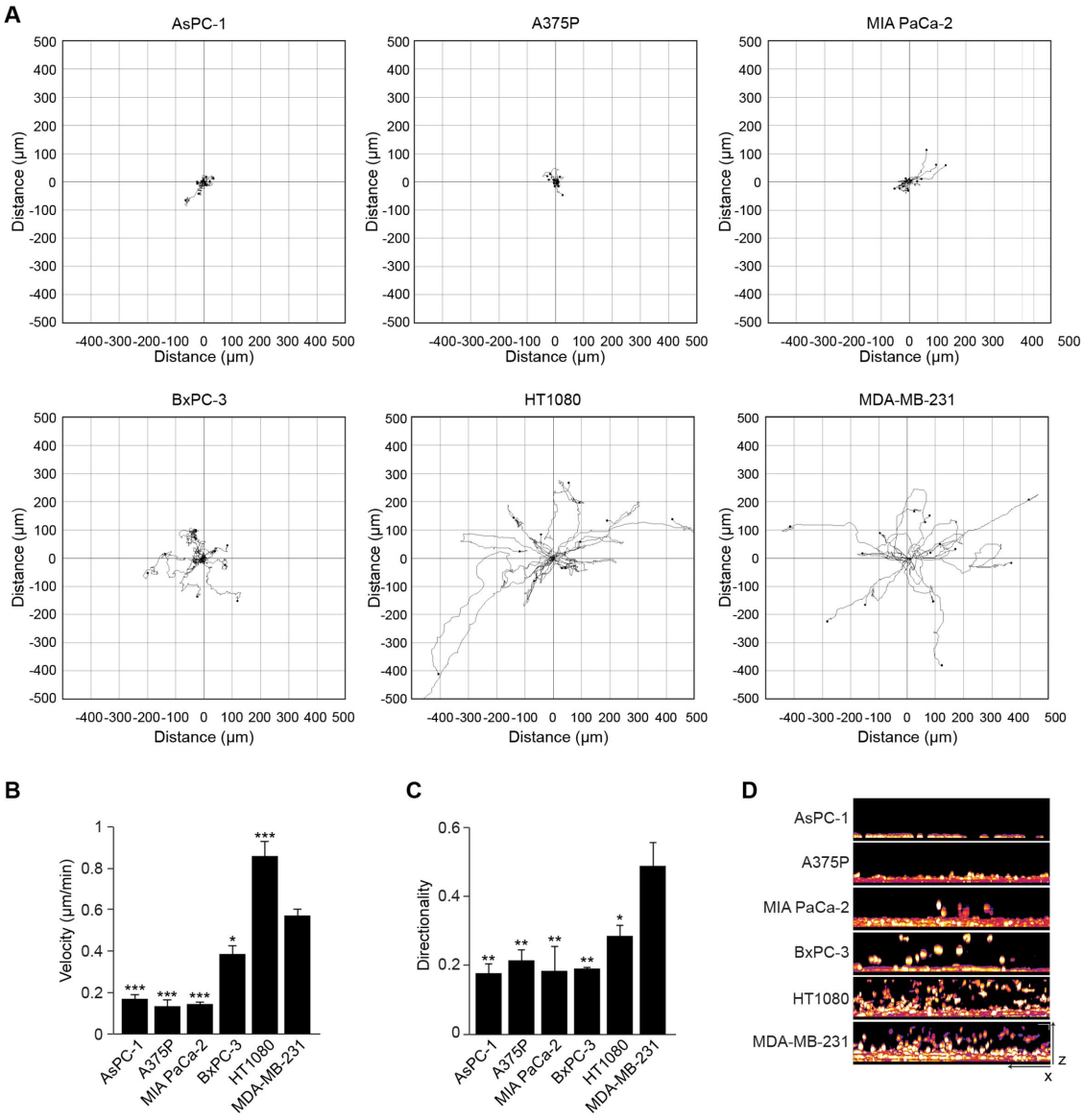

FIGURE 2: Hic-5 expression level correlates with 3D cell migration and in vitro invasiveness. (A) Representative migration tracks of the cancer cell lines migrating in 3D cell-derived matrices (CDMs) for a period of 16 h. (B) Velocity and (C) directionality of the cancer cell lines in 3D CDMs (n = at least 45 cells). (D) Images of the cancer cell lines invading through dense collagen/fibronectin gels. Data represent mean ± SEM of at least three independent experiments. One-way ANOVA using Dunnet's multiple comparison test was performed. *, $p < 0.05$; **, $p < 0.01$, and ***, $p < 0.001$.

for influencing the distinct 3D cell morphologies, we transiently expressed either GFP-Hic-5 or GFP-Hic-5 with single deletions in the LD1, LD2, or LD3 motifs, as well as a Y38/60F nonphosphorylatable mutant (Hetey *et al.*, 2005) in MDA-MB-231 cells (Figure 5, A and B). MDA-MB-231 cells expressing these mutants were seeded into 3D CDMs, as well as onto micropatterned lines to evaluate their respective morphologies. When seeded on either substrate, cells overexpressing the full-length GFP-Hic-5 wild type (WT) were highly elongated or "hypermesenchymal" as compared with the GFP-expressing control cells (Figure 5, C–E). However, cells overexpressing GFP-Hic-5 ΔLD1, ΔLD2, or ΔLD3 mutants were unable to replicate this hypermesenchymal phenotype (Figure 5, D and E), indicating that these motifs are crucial for the ability of Hic-5 to regulate 3D/1D mesenchymal morphology. Additionally, cells expressing the Hic-5 nonphosphorylatable mutant Y38/60F also had a reduced ability to promote a hypermesenchymal phenotype in both 3D CDMs and on fibronectin lines (Figure 5, D and E).

A similar domain analysis was performed for paxillin by transiently expressing GFP-paxillin containing single deletions of LD1, LD2, and LD4 motifs as well as the Y31/118F nonphosphorylatable mutant (Bellis *et al.*, 1995; Hildebrand *et al.*, 1995; Zaidel-Bar *et al.*, 2007) in MDA-MB-231 cells (Figure 5, F and G). When seeded into 3D CDMs and on fibronectin-coated lines, cells overexpressing GFP-paxillin WT or the ΔLD1 mutant shifted toward a more rounded phenotype, as compared with GFP-expressing control cells (Figure 5, H–J). However, cells expressing the GFP-paxillin ΔLD2 or ΔLD4 mutants were unable to promote this rounded phenotype (Figure 5, I and J), suggesting that the paxillin LD2 and LD4 motifs regulate the switch to an amoeboid morphology, while the LD1 motif is dispensable. Furthermore, the paxillin Y31/118F nonphosphorylatable

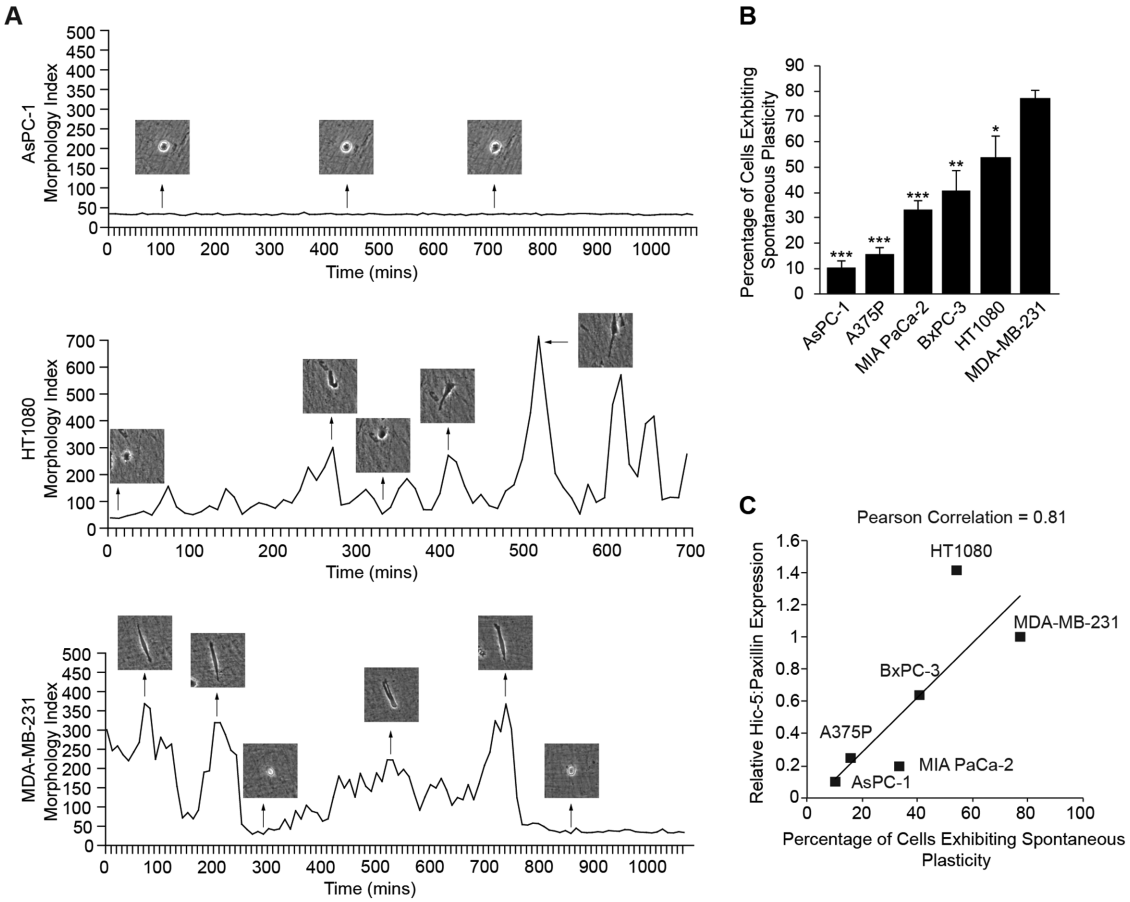

FIGURE 3: Hic-5 expression correlates with 3D morphological plasticity. (A) Phase contrast time-lapse images of the morphology in 3D cell-derived matrices (CDMs) of individual AsPC-1, HT1080, and MDA-MB-231 cells. (B) Quantitation of the percent of cells exhibiting spontaneous plasticity in each of the indicated cancer cell lines over a period of 16 h (n = at least 45 cells). (C) Correlation of the relative Hic-5 to paxillin expression ratio to spontaneous plasticity exhibited by the indicated cancer cell lines. Data represent mean ± SEM of at least three independent experiments. One-way ANOVA using Dunnet's multiple comparison test was performed. *, $p < 0.05$; **, $p < 0.01$; and ***, $p < 0.001$.

mutant was also unable to induce a more rounded phenotype (Figure 5, I and J), indicating that phosphorylation of paxillin at Y31/118 is also necessary for paxillin to stimulate a mesenchymal to amoeboid transition. Importantly, these major changes in cell phenotype are specific for cells plated on 3D/1D matrices because all of the Hic-5, and paxillin mutants targeted as efficiently as the WT proteins to focal adhesions in cells spread onto a 2D fibronectin substrate, indicating that each mutant retained this critical aspect of their functionality (Supplemental Figure S1).

Ectopic expression of Hic-5 is sufficient to induce a mesenchymal phenotype and promote plasticity and invasion in A375MEA-3 melanoma cells

To further explore the potential role of Hic-5 as a primary driver of cancer cell mesenchymal phenotype, we evaluated the ability of ectopically expressed GFP-Hic-5 to induce a change in 3D cell morphology when introduced into low Hic-5–expressing A375MEA-3 melanoma cells (Xu *et al.*, 2008). A375MEA-3 cells, consistent with their low Hic-5 expression relative to MDA-MB-231 cells and a corresponding Hic-5:paxillin ratio of 0.28, typically display a primarily rounded morphology when plated into 3D CDMs, forming very few, small focal adhesions (Figure 6, A–C, and unpublished data). GFP-expressing cells retained this rounded morphology when plated in 3D CDMs (Figure 6D, top-left panel). In contrast, transient introduction of GFP-Hic-5 into the A375MEA-3 cells resulted in a significant increase in the percentage of cells that exhibited a more elongated, mesenchymal phenotype with prominent GFP-Hic-5–containing cell–ECM adhesions (Figure 6, D–F and I). Furthermore, the propensity to exhibit plasticity and switch between phenotypes in 3D CDMs, as well as the ability of these cells to invade through Matrigel, also increased following the introduction of GFP-Hic-5 (Figure 6, G, H, and J). Similar phenotypic changes were obtained following ectopic expression of GFP-Hic-5 in the A375P melanoma cell line (Supplemental Figure S2), which has a similar Hic-5:paxillin expression ratio of 0.24 (Figure 1D). However, AsPC-1 cells, which have almost no detectable endogenous Hic-5 (Figure 1A), were unresponsive to the introduction of Hic-5, suggesting that certain rounded/amoeboid cell lines have lost their capacity to form stable 3D adhesions. Importantly, as with the other cancer lines including the A375P and AsPC-1 cells, when plated on 2D substrates, A375MEA-3 cells expressing either GFP or GFP-Hic-5 WT, were able to spread equally well and both formed robust focal adhesions (Figure 6D, right panels). To determine if the Hic-5 LD motifs and Y38/60 phosphorylation sites are also essential for driving a mesenchymal phenotype in this cell line as in the MDA-MB-231 cells, we transfected the A375MEA-3 cells with the respective GFP-Hic-5 constructs. In contrast to the GFP-Hic-5–expressing cells, cells expressing the LD deletion mutants, as well as the nonphosphorylatable

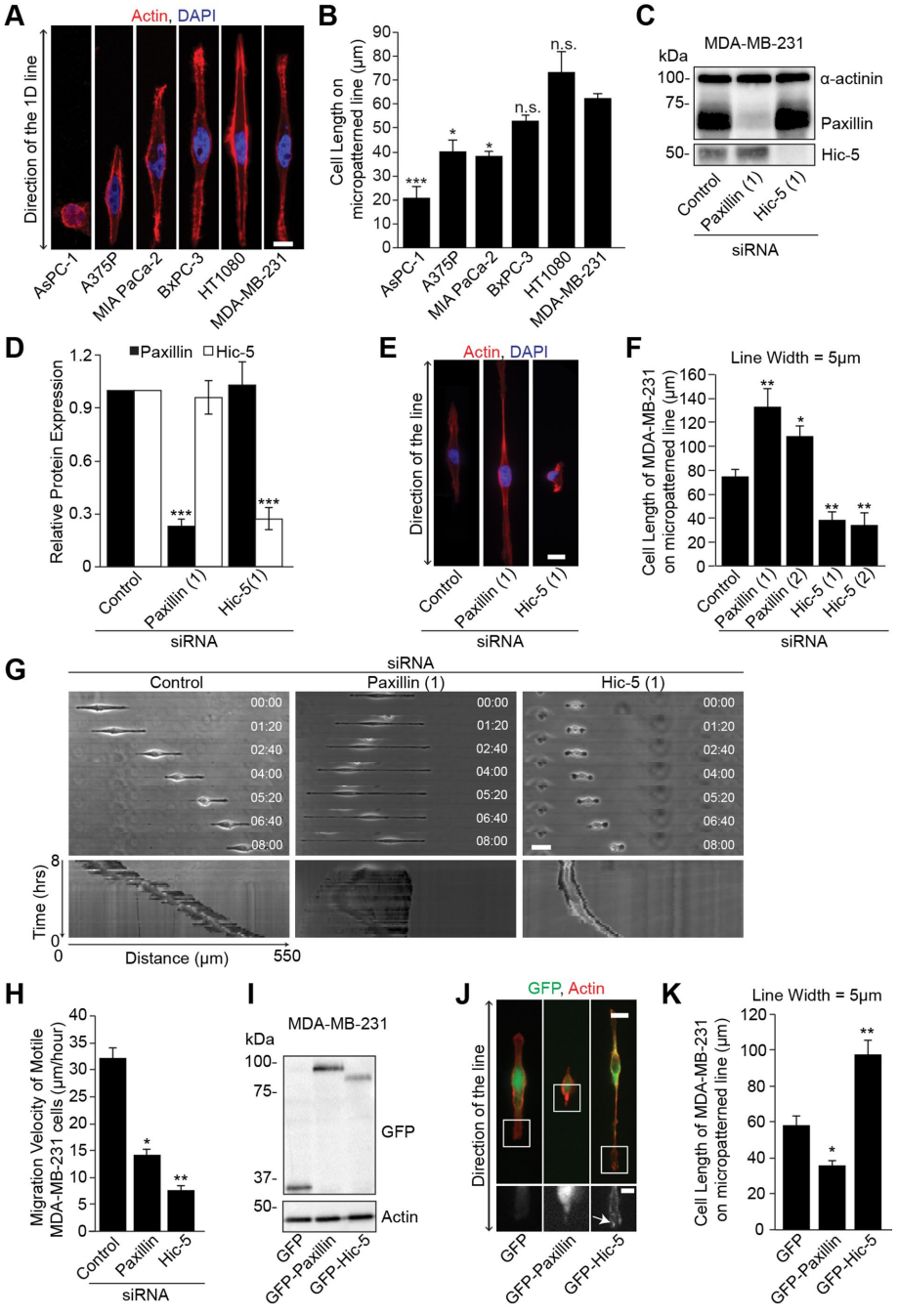

FIGURE 4: Hic-5 and paxillin inversely regulate cell morphology and one-dimensional (1D) migration on micropatterned substrates. (A) Representative images of various cancer cell lines on 5 μm fibronectin-coated micropatterned lines. Scale bar = 10 μm. (B) Quantitation of the average length of cells spread on the fibronectin lines (n = at least 80 cells). Data represent mean ± SEM of three independent experiments. One-way ANOVA using Dunnet's multiple comparison test was performed. (C) Western blot of cell lysates from RNAi-mediated knockdown of paxillin or Hic-5 in MDA-MB-231 cells. (D) Quantitation of the relative levels of paxillin or Hic-5 post siRNA treatment. (E) Immunofluorescence of MDA-MB-231 cells plated on the lines post RNAi-mediated knockdown. Scale bar = 10 μm. (F) Quantitation of the average length of MDA-MB-231 cells spread along the lines post RNAi-mediated knockdown using two different oligonucleotides for paxillin and Hic-5 (n = at least 100 cells). (G) Time-lapse images of 1D migration (top row) of paxillin or Hic-5 knockdown cells as compared with control MDA-MB-231 cells, over a period of 8 h, along with respective kymographs (bottom row). Scale bar = 20 μm. (H) Quantitation of the 1D migration velocity along the fibronectin lines post siRNA treatment (n = at least 20 cells). (I) Western blot of cell lysates of MDA-MB-231 cells expressing GFP, GFP-paxillin, or GFP-Hic-5. (J) Immunofluorescence imaging of cells expressing GFP, GFP-paxillin, or GFP-Hic-5 spread on fibronectin lines. Insets (and arrowhead) showing the presence of GFP-Hic-5–positive focal adhesions. Scale bar = 10 μm; inset = 5 μm. (K) Quantitation of average cell length of MDA-MB-231 cells expressing GFP, GFP-paxillin, or GFP-Hic-5 (n = at least 90 cells). Data represent mean ± SEM of at least three independent experiments. A two-tailed unpaired Student's t test was performed. *, $p < 0.05$; **, $p < 0.01$; and ***, $p < 0.001$.

mutant remained rounded and had lower abilities to switch phenotypes, similar to the parental cells (Figure 6, I and J). It is well established that Rac1 activity is important for 3D mesenchymal cell motility (Sanz-Moreno *et al.*, 2008) and Rac1 activity is modestly reduced in the rounded MDA-MB-231 cells following RNAi knockdown of Hic-5 (Deakin and Turner, 2011). Accordingly, pharmacologic inhibition of Rac1 caused the GFP-Hic-5–expressing A375MEA-3 cells to revert back to an amoeboid phenotype (Figure 6K). Together, these data indicate that Hic-5 overexpression in cell lines such as A375MEA-3 and A375P cells is sufficient to drive a shift toward a Rac1-mediated mesenchymal morphology in 3D ECM and to promote phenotypic plasticity and invasion. Furthermore, mutant analysis in MDA-MB-231 and A375MEA-3 cells indicates that the LD1, LD2, and LD3 motifs as well as the Y38/60 phosphorylation sites of Hic-5 are required for this behavior.

The activity of vinculin is necessary for Hic-5–driven amoeboid to mesenchymal transition in 3D matrices

Hic-5 and paxillin function primarily as adaptor proteins, with interactions between their respective LD motifs and tyrosine phosphorylation sites and various structural and signaling proteins controlling cytoskeletal remodeling (Brown and Turner, 2004; Deakin and Turner, 2008). Interestingly, although they share several common LD binding partners such as FAK and vinculin (Turner *et al.*, 1990; Burridge *et al.*, 1992; Bellis *et al.*, 1995; Thomas *et al.*, 1999), our mutation analysis (Figure 5) indicated that deletion of their respective LD motifs resulted in drastically different 3D cell morphologies. We therefore performed proximity ligation assay (PLA) analysis to determine whether differential interactions with these two proteins could account for the observed phenotypes. Interestingly, although the number of PLA spots between Hic-5 and pY397FAK was lower than between paxillin and pY397FAK, in both amoeboid and mesenchymal cell phenotypes (unpublished data), there was no significant difference in the respective

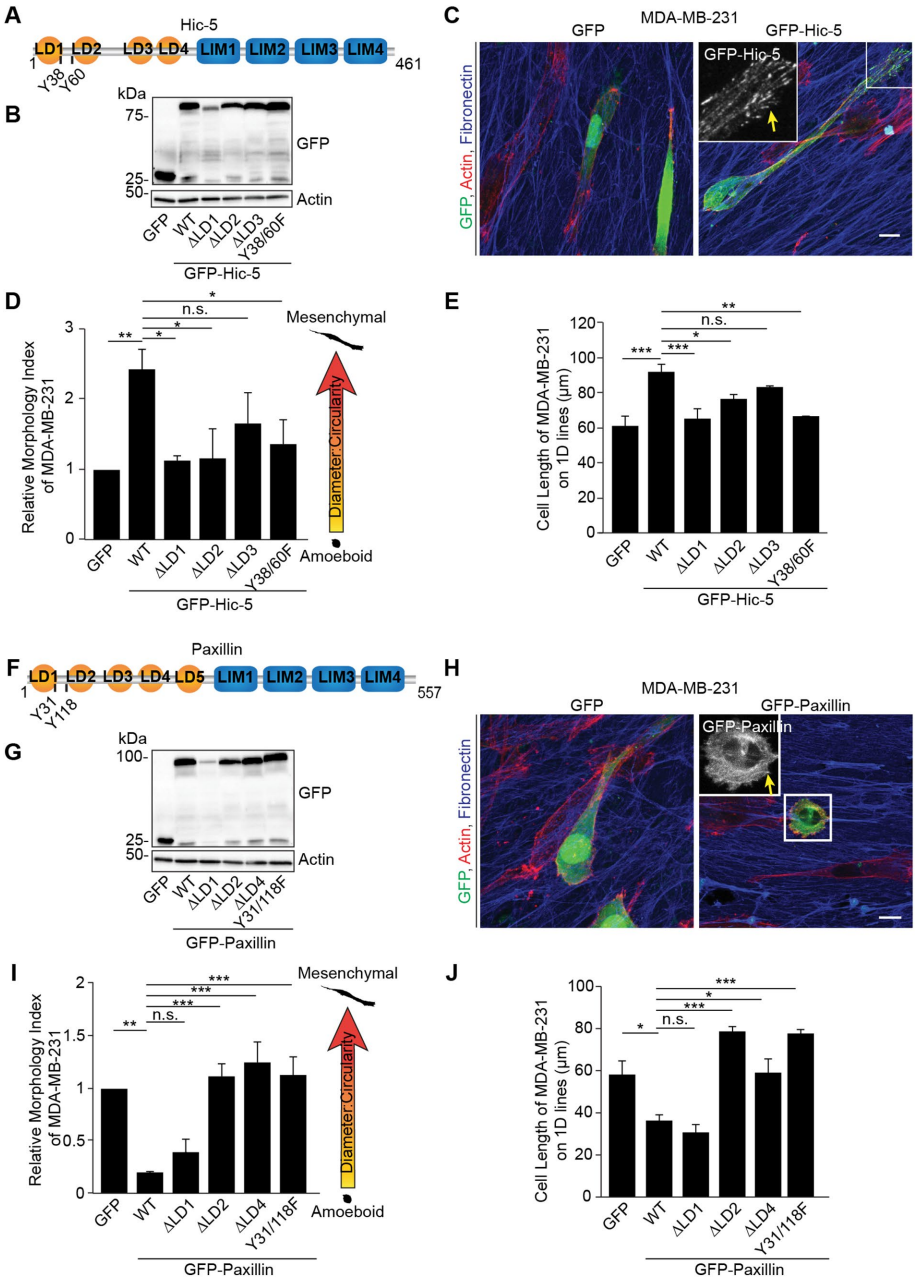

FIGURE 5: Distinct LD motifs and phosphorylation sites within Hic-5 and paxillin influence 3D cancer cell morphology. (A) Schematic of Hic-5 domain structure indicating LD motifs and LIM domains, as well as the principal tyrosine phosphorylation sites. (B) Western blot of lysates of MDA-MB-231 cells expressing GFP, GFP-Hic-5 WT, GFP-Hic-5 ΔLD1, ΔLD2, ΔLD3, and the Y38/60 nonphosphorylatable mutants. (C) Immunofluorescence images of cells expressing GFP and GFP-Hic-5 WT in 3D CDMs. Inset showing GFP-Hic-5–positive adhesions. Scale bar = 10 μm. (D) Quantitation of the morphology index of cells expressing GFP-Hic-5 WT and mutants relative to the GFP-expressing cells (n = at least 30 cells). (E) Quantitation of the average cell length of cells expressing GFP-Hic-5 WT and mutants plated on fibronectin micropatterned lines (n = at least 30 cells). (F) Schematic of paxillin domain structure indicating LD motifs and LIM domains, as well as the principal tyrosine phosphorylation sites. (G) Western blot of lysates of MDA-MB-231 cells expressing GFP, GFP-paxillin WT, GFP-paxillin ΔLD1, ΔLD2, ΔLD4, and the Y31/118F nonphosphorylatable mutants. (H) Immunofluorescence images of cells expressing GFP and GFP-paxillin WT in 3D CDMs. Scale bar = 10 μm. (I) Quantitation of the morphology index of cells expressing GFP-paxillin WT and mutants relative to the GFP-expressing cells (n = at least 30 cells). (J) Quantitation of the average length of cells expressing GFP-paxillin WT and mutants plated on fibronectin-coated micropatterned lines (n = at least 30 cells). One-way ANOVA using Dunnet's multiple comparison test was performed. Data represent mean ± SEM of at least three independent experiments. *, $p < 0.05$; **, $p < 0.01$; and ***, $p < 0.001$.

ratios (Supplemental Figure S3), indicating that the relative interaction of FAK with Hic-5 or paxillin did not change significantly in mesenchymal versus amoeboid cells and is therefore not likely to be the principal mechanism controlling 3D cell morphology. Unfortunately, attempts to perform PLA with the available vinculin antibodies were unsuccessful.

Previous reports indicate that vinculin can influence the directionality and persistence of mesenchymal cells migrating in 3D CDMs and collagen gels (Thievessen *et al.*, 2015; Rahman *et al.*, 2016). However, the mechanism by which vinculin regulates 3D morphology is still not known. We therefore examined how the activity of vinculin might influence cancer cell phenotype and plasticity in 3D ECM downstream from Hic-5. Accordingly, YFP-tagged full-length vinculin (WT), a constitutively active talin-binding mutant (T12) and a mutant of vinculin with reduced affinity for talin (A50I; Humphries *et al.*, 2007) were each transiently expressed in MDA-MB-231 cells plated into 3D CDMs (Figure 7, A–C). The active YFP-vinculin T12 mutant-expressing cells exhibited a predominantly hypermesenchymal phenotype (Figure 7, B and D), had reduced plasticity (Figure 7E), similar to Hic-5 overexpressing MDA-MB-231 cells (Figure 4; Deakin and Turner, 2011), and stimulated the formation of robust adhesions (Figure 7B) that colocalized with Hic-5 (Supplemental Figure S4A, upper panel). In contrast, YFP-vinculin A50I-expressing MDA-MB-231 cells were predominantly rounded, had a reduced ability to switch phenotypes and also had shorter cell lengths on the fibronectin-coated micropatterned lines as compared with WT vinculin (Figure 7, B and D–F). These data suggest that vinculin activation is required for promoting the formation and stabilization of adhesions in 3D and thereby promoting a mesenchymal phenotype in the MDA-MB-231 cells.

Finally, to assess whether there is a causal relationship between Hic-5 expression and vinculin signaling, we evaluated whether overexpression of the active vinculin mutant was sufficient to stimulate a mesenchymal phenotype independent of Hic-5 by transiently transfecting the active YFP-vinculin T12 mutant into A375MEA-3 cells plated into 3D CDMs. Interestingly, unlike the MDA-MB-231 cells, which became hypermesenchymal with the expression of this mutant, the A375MEA-3 cells retained a predominantly rounded phenotype, but still formed robust focal adhesions (Figure 7, G and H), indicating that active vinculin is not sufficient to promote a mesenchymal

phenotype in the absence of sufficient Hic-5. A similar result was obtained following knockdown of Hic-5 in MDA-MB-231 cells along with expression of YFP-vinculin T12 mutant, further supporting this conclusion (Supplemental Figure S4). Additionally, A375MEA-3 cells coexpressing the YFP-vinculin A50I mutant along with RFP-Hic-5 retained their predominantly amoeboid morphology (Figure 7, G and H). Given that Hic-5 cannot efficiently interact with vinculin A50I (Deakin *et al*., 2012a), the data support a mechanism by which interaction between Hic-5 and vinculin is necessary for Hic-5's ability to stimulate a 3D mesenchymal phenotype.

DISCUSSION

Individual cancer cells can utilize either an amoeboid or a mesenchymal mode of migration to translocate through 3D matrices (Wolf *et al*., 2003a; Pankova *et al*., 2010). Spontaneous switching between the two modes of migration or "plasticity" represents one of the primary reasons by which some highly invasive cancer cells can evade MMP-targeted therapeutic intervention (Friedl and Wolf, 2003). Hence, there is a clinical need to identify prognostic indicators of each mode of tumor cell migration and to decipher the fundamental mechanisms underlying phenotypic plasticity to help identify appropriate treatment options. We have previously shown that experimental manipulation of the respective levels of the closely related focal adhesion adaptor proteins paxillin and Hic-5 in the highly invasive MDA-MB-231 breast cancer cell line produces profound shifts in cell migratory phenotype, plasticity, and invasion in 3D matrix environments. Specifically, Hic-5 knockdown resulted in a predominantly rounded/amoeboid morphology, whereas paxillin depletion shifted the cells to a hypermesenchymal phenotype indicating that a balance of Hic-5 to paxillin expression and signaling was required (Deakin and Turner, 2011). In the current study, we tested the hypothesis that the endogenous levels of these two proteins as well as their relative expression may be used to predict the predominant mode of 3D migration of different cancer cell populations.

Analysis of an array of cancer cell lines, derived from several different tumor types including melanoma, pancreatic, fibrosarcoma, and breast cancer revealed widely varying levels of Hic-5 expression, which closely corresponded to the cell line's respective 3D morphology and degree of invasiveness in vitro, whereas the level of paxillin across all cell lines was more constant (Figures 1 and 2). The cancer cell lines with the lowest endogenous Hic-5 levels and thus low Hic-5:paxillin ratio exhibited a predominantly rounded morphology and lacked the ability to switch effectively to the mesenchymal phenotype, whereas cell lines with the highest levels of Hic-5 expression and a correspondingly high Hic-5:paxillin ratio, presented with a mixture of amoeboid and mesenchymal morphologies and also exhibited the greatest capacity to undergo phenotypic amoeboid to mesenchymal switching and to invade through dense 3D collagen–fibronectin matrices (Figures 1–3). Thus, we conclude that the level of Hic-5 can serve as a primary indicator of tumor cell migratory behavior and its increased expression drives the shift from an amoeboid toward a mesenchymal phenotype, facilitates plasticity and cancer cell invasiveness. In contrast, paxillin expression in and of itself is a relatively poor indicator of cancer cell phenotype, but nevertheless serves an essential role in enabling plasticity from mesenchymal to amoeboid morphologies. Indeed, to date we have been unable to identify any cancer cell lines that express either low levels or no paxillin in relation to Hic-5, perhaps because paxillin is required for long-term cell viability.

The formation and stabilization of integrin-based ECM adhesions is one of the main molecular mechanisms underlying an amoeboid to mesenchymal transition in 3D (Wolf and Friedl, 2006; Pankova *et al*., 2010). Remarkably, the selective influence of Hic-5 expression on 3D cell morphology and associated formation of 3D adhesions (Figures 5 and 6; Deakin and Turner, 2011) does not carry over to a 2D matrix environment, where all cells examined exhibited a well-spread morphology with abundant focal adhesions regardless of their Hic-5 expression levels (Figure 1), emphasizing a unique role for Hic-5 in 3D adhesion formation and stabilization. However, plating the cells on narrow, micropatterned "1D" lines of fibronectin, which has been reported to mimic 3D motility on ECM bundles (Doyle *et al*., 2009), revealed a similar dependence on Hic-5 expression, with high Hic-5–expressing cells exhibiting a more elongated morphology and positive focal adhesion staining as compared with low endogenous Hic-5–expressing cells or MDA-MB-231 cells following Hic-5 RNAi knockdown (Figure 4). Although paxillin is one of the earlier proteins to be recruited to 2D cell–ECM adhesion sites (Zaidel-Bar *et al*., 2003; Ballestrem *et al*., 2006), based on our current observations, paxillin is clearly not sufficient to stimulate adhesion formation in the absence of Hic-5 in either a 3D ECM or on 1D micropatterned lines (Figures 1 and 4). Conversely, the mesenchymal to amoeboid switch most likely requires paxillin-dependent regulation of adhesion disassembly, most likely via regulation of FAK signaling, as we and others have previously reported (Zaidel-Bar *et al*., 2007; Deakin and Turner, 2011).

Significantly, introduction of GFP-Hic-5 into A375MEA-3 or A375P melanoma cells, which both express low levels of endogenous Hic-5, was sufficient to cause a significant shift in their overall morphology toward a more mesenchymal phenotype, enabled more cells to exhibit plasticity, and stimulated invasion (Figure 6). These data complement and extend previous observations linking Hic-5 up-regulation to increased cell invasiveness through the formation of matrix degrading invadopodia during epithelial to mesenchymal transition in response to TGF-β (Tumbarello and Turner, 2007; Pignatelli *et al*., 2012). This process is considered analogous to events associated with tumor progression and increased malignancy and raises the intriguing possibility that increased TGF-β secretion and signaling within the tumor microenvironment (Derynck *et al*., 2001; Bhowmick *et al*., 2004), for example by cancer associated fibroblasts (CAFs), could influence tumor cell malignancy by stimulating the tumor cells to increase Hic-5 expression. Interestingly, we have recently shown that Hic-5 is also up-regulated in the CAFs to promote stromal matrix deposition and remodeling, which can further influence tumor cell invasion via a non–cell autonomous manner (Goreczny *et al*., 2016, 2018). Importantly, Hic-5 up-regulation has been linked with various human cancers including osteosarcoma, lung adenocarcinoma, as well as breast and prostate carcinomas (Mestayer *et al*., 2003; Azuma *et al*., 2005; Mackinnon *et al*., 2011; Goreczny *et al*., 2016). Further studies will be required to dissect the respective roles of Hic-5 up-regulation in the tumor cells versus the CAFs in determining patient outcome.

Paxillin and Hic-5 contain highly conserved LD motifs, phosphorylation sites, and LIM domains (Figures 5 and 6) that function as docking sites for several signaling proteins, including FAK and vinculin (Tumbarello *et al*., 2002; Brown and Turner, 2004). Through our domain mapping studies, we have now identified several of the LD motifs and tyrosine phosphorylation sites of both Hic-5 and paxillin as being required for their respective regulation of 3D cell morphology (Figures 5 and 6), suggesting the involvement of multiple binding partners. Interestingly, although the PLA analysis demonstrated that active pY397FAK interacted with both Hic-5 and paxillin, we saw no significant shift in the ratio of their respective interactions in amoeboid versus mesenchymal cell phenotypes (Supplemental Figure S3), suggesting that differential binding of, or signaling

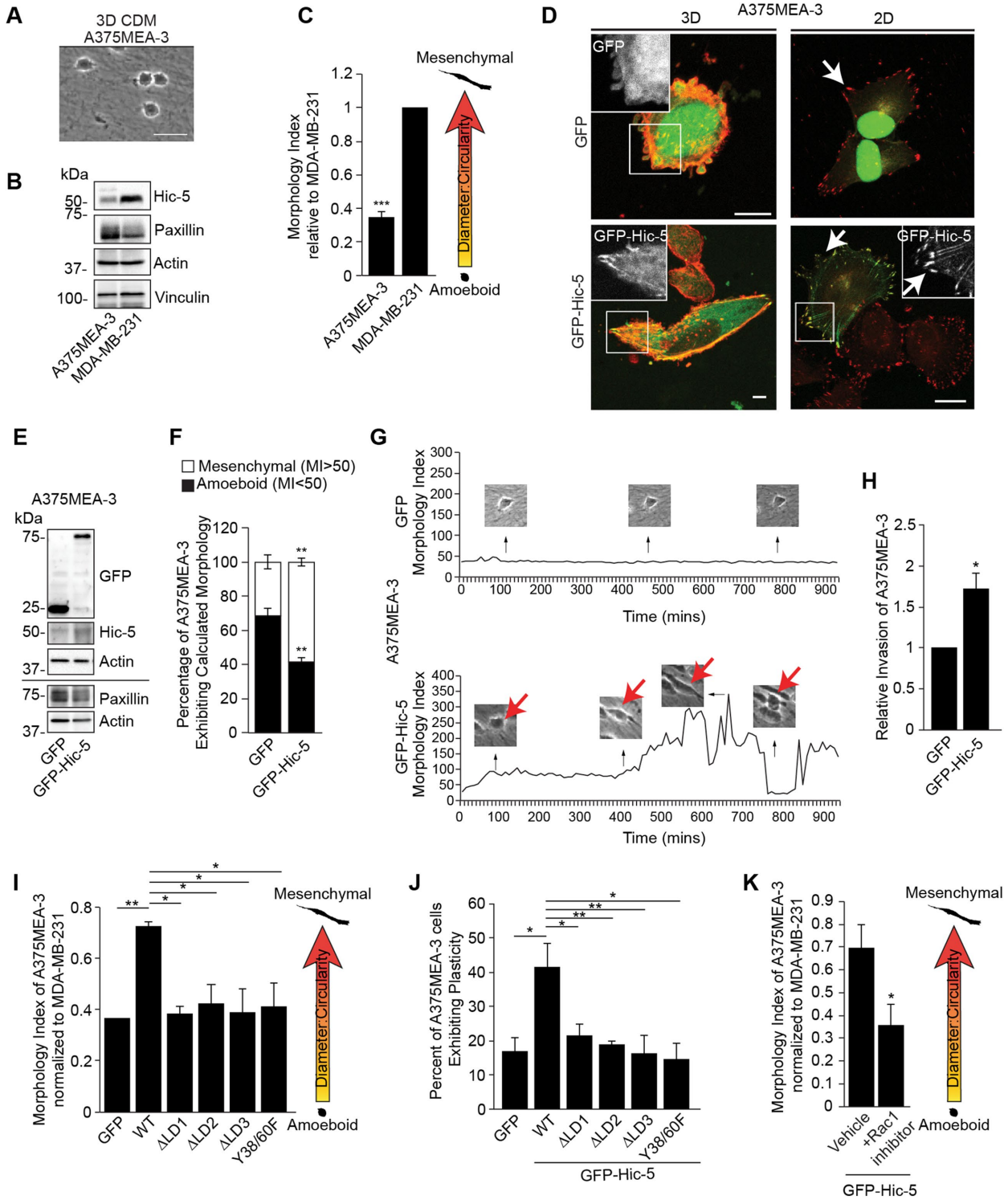

FIGURE 6: Ectopic expression of Hic-5 is sufficient to induce a mesenchymal phenotype and promote plasticity and invasion in A375MEA-3 melanoma cells. (A) Representative phase contrast image of parental A375MEA-3 cells in 3D CDMs. Scale bar = 50 μm. (B) Western blot of lysates from A375MEA-3 vs. MDA-MB-231 cells showing respective levels of endogenous Hic-5, paxillin, and vinculin. (C) Quantitation of the morphology index of parental A375MEA-3 relative to MDA-MB-231 cells (n = at least 25 cells). (D) Images of A375MEA-3 cells expressing GFP or GFP-Hic-5 WT in 3D CDMs (left) and 2D fibronectin (right). Scale bar = 10 μm (left) and 25 μm (right). (E) Western blot of A375MEA-3 cells expressing GFP or GFP-Hic-5 WT. (F) Quantitation of the percentage of amoeboid or mesenchymal cells calculated based on their morphology index (n = at least 25 cells). (G) Phase contrast time-lapse images of the plasticity exhibited by the A375MEA-3 cells expressing GFP or GFP-Hic-5 WT over a period of 16 h. (H) Quantitation of the relative invasion through Matrigel of A375MEA-3 cells expressing GFP or GFP-Hic-5 WT (n = at least 200 cells). Data represent mean ± SEM of three independent experiments. A two-tailed unpaired Student's t test was performed. (I) Quantitation of the morphology index of A375MEA-3 cells expressing GFP-Hic-5 WT, ΔLD1, ΔLD2, ΔLD3, or Y38/60F nonphosphorylatable

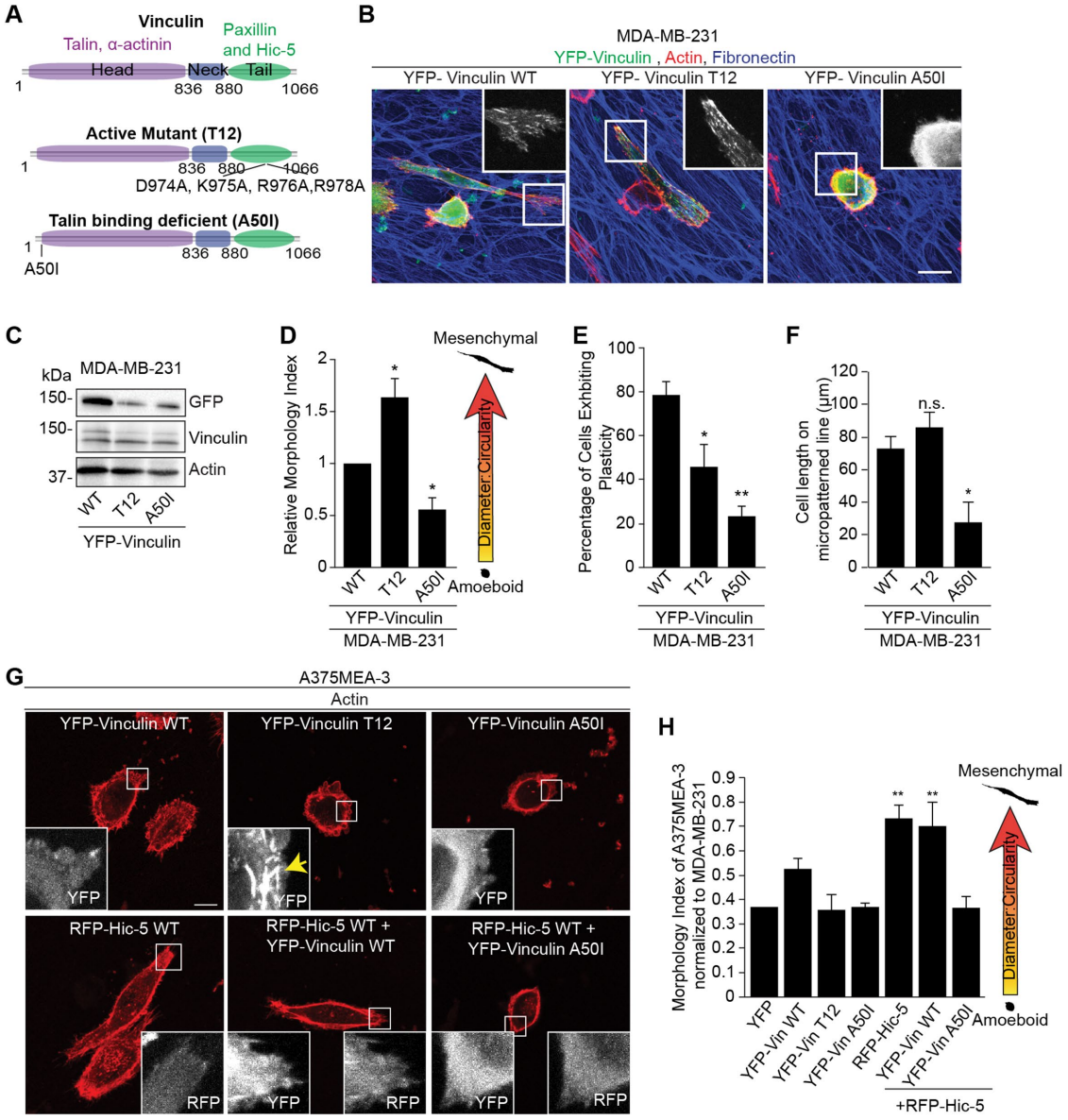

FIGURE 7: The activity of vinculin in addition to interaction with Hic-5 drives the amoeboid to mesenchymal transition in cancer cells in 3D matrices. (A) Schematic showing vinculin head, neck, and tail domains, as well as the vinculin T12 and A50I mutants. (B) Images of MDA-MB-231 cells expressing YFP-vinculin WT, T12, or A50I mutants spread in 3D CDMs. Insets show distribution of YFP-vinculin WT, T12, and A50I within the cells. Scale bar = 20 μm. (C) Western blot of MDA-MB-231 cells expressing YFP-vinculin WT, T12, or A50I mutants. (D) Quantitation of the morphology index of MDA-MB-231 cells expressing YFP-vinculin T12 and A50I mutants relative to YFP-vinculin WT-expressing cells (n = at least 30 cells). (E) Quantitation of the percentage of cells exhibiting morphological plasticity over a period of 16 h (n = at least 30 cells). (F) Quantitation of cell length of MDA-MB-231 cells expressing YFP-vinculin WT, T12, or A50I spread on fibronectin-coated micropatterned lines (n = at least 30 cells). Data represent mean ± SEM of three independent experiments. A two-tailed unpaired Student's t test was performed. (G) Images of A37MEA-3 cells in 3D CDMs expressing YFP-vinculin mutants and RFP-Hic-5. Scale bar = 10 μm. (H) Quantitation of the morphology index of A375MEA-3 cells expressing YFP-vinculin mutants and RFP-Hic-5 (n = at least 25 cells). The morphology index for the A375MEA-3 cells has been normalized to the morphology index of MDA-MB-231 cells. Data represent mean ± SEM of at least three independent experiments. One-way ANOVA using Dunnet's multiple comparison test was performed. *, $p < 0.05$ and **, $p < 0.01$.

mutants, relative to GFP-expressing cells (n = 30 cells). The morphology index for the A375MEA-3 cells has been normalized to the morphology index of MDA-MB-231 cells. (J) Quantitation of the percentage of cells exhibiting plasticity over a period of 16 h (n = at least 25 cells). Data represent mean ± SEM of three independent experiments. A one-way ANOVA with Dunnet's multiple comparison test was used. (K) Quantitation of the relative morphology index of GFP-Hic-5 A375MEA-3 cells treated with vehicle or Rac1 inhibitor (n = at least 30 cells), normalized to the morphology index of MDA-MB-231 cells. Data represent mean ± SEM of three at least independent experiments. A two-tailed unpaired Student's t test was performed. *, $p < 0.05$; **, $p < 0.01$; and ***, $p < 0.001$.

through FAK-paxillin versus FAK-Hic-5 is unlikely to be the primary signaling axis that can account for the Hic-5–driven mesenchymal phenotype. Furthermore, our previous studies demonstrated that FAK inhibition in MDA-MB-231 cells produced a hypermesenchymal phenotype, comparable to paxillin depletion, with the formation of robust vinculin-positive adhesions (Deakin *et al.*, 2012a), implicating vinculin rather than FAK in promoting a 3D mesenchymal morphology. Recently, we showed that Hic-5 interacts with tensin1 to promote fibrillar adhesion formation (Goreczny *et al.*, 2018). Thus, the potential role of this interaction in Hic-5's ability to promote mesenchymal cell migration warrants further investigation.

The role of vinculin in regulating force transmission and strengthening of adhesions in 2D has been extensively studied (Cohen *et al.*, 2006; Humphries *et al.*, 2007; Dumbauld *et al.*, 2013). Importantly, although paxillin was previously found to interact with vinculin in Rac1-driven focal complexes in 2D matrices, vinculin was shown to interact preferentially with Hic-5 in 3D adhesions (Deakin *et al.*, 2012a). Furthermore, paxillin depletion also induced robust vinculin and Hic-5–positive 3D adhesions in the resulting hypermesenchymal MDA-MB-231 cells (Deakin and Turner, 2011). Vinculin has been shown to influence directionality and persistence in mesenchymal cells in 3D CDMs (Rahman *et al.*, 2016) and vinculin null fibroblasts exhibit a rounded morphology when plated into 3D collagen gels (Thievessen *et al.*, 2015). We have now shown that in MDA-MB-231 cells, expression of a vinculin mutant (A50I) with reduced affinity for talin phenocopies Hic-5 depletion in these cells by shifting the cells to a primarily rounded morphology (Figure 7). Conversely, expression of the active vinculin T12 mutant stimulated a hypermesenchymal phenotype with robust focal adhesions supporting the notion that vinculin activation as well as Hic-5 expression is required for the acquisition of a mesenchymal phenotype in 3D CDMs.

Interestingly, in contrast to Hic-5 overexpression, introduction of the active vinculin T12 mutant into the low Hic-5–expressing A375MEA-3 cells was not sufficient to generate a shift toward a more mesenchymal morphology even though it stimulated the formation of robust focal adhesions (Figure 7), most likely via talin binding and subsequent clustering of active integrins (Humphries *et al.*, 2007). On the other hand, coexpression of Hic-5 with the vinculin A50I mutant in these cells blocked Hic-5's ability to promote the mesenchymal phenotype indicating that Hic-5 expression, coupled with vinculin binding and activation is required to coordinate downstream signaling to promote both Rac1-driven cell protrusions and focal adhesion formation and stabilization. Furthermore, in contrast to Hic-5, paxillin has been shown to interact with the vinculin A50I mutant at the plasma membrane (Deakin *et al.*, 2012a; Case *et al.*, 2015), which could provide a mechanism by which paxillin stimulates focal adhesion disassembly and switching to an amoeboid phenotype in 3D ECM.

RhoA and Rac1 activity is tightly linked to 3D amoeboid and mesenchymal morphologies, respectively (Sanz-Moreno *et al.*, 2008; Deakin and Turner, 2011). Hic-5 can regulate both Rac1 and RhoA GTPase activity by interacting with several GEFs and GAPs (Turner *et al.*, 1999; Tumbarello *et al.*, 2002; Tumbarello *et al.*, 2005; Yu *et al.*, 2010). Additionally, tyrosine phosphorylated Hic-5 has been shown to regulate Rac1 activity to promote invasion (Hetey *et al.*, 2005; Pignatelli *et al.*, 2012), and our current results indicate that phosphorylation of Hic-5 is essential for Hic-5's ability to drive a mesenchymal phenotype. Moreover, the activity of Rac1 has been shown to promote a vinculin-Arp2/3 interaction that drives actin polymerization and membrane protrusions in mesenchymal cells (DeMali *et al.*, 2002; Yamazaki *et al.*, 2009). Interestingly, our data using the Rac1 inhibitor (Figure 6) demonstrate that Rac1-driven protrusive activity is essential for Hic-5 overexpression to induce a mesenchymal phenotype in the A375MEA-3 cells. The fact that Rac1 and RhoA activity can also influence the interaction of vinculin with Hic-5 and paxillin in 2D as well as 3D matrices (Deakin *et al.*, 2012a), indicates that this balance of RhoGTPase signaling and competition for vinculin by Hic-5 and paxillin represent a core component of morphological plasticity regulation. Identification of the specific GEFs and GAPs that are controlled by Hic-5 and how their expression correlates with Hic-5 expression in human tumors will likely be a productive line of future study. In conclusion, we have identified Hic-5 expression as a key determinant of cancer cell morphology and plasticity during 3D migration and thus it, in combination with the relative Hic-5:paxillin ratio, may serve as a useful predictive indicator of tumor malignancy and mode of invasion to facilitate the selection of appropriate therapeutic intervention strategies.

MATERIALS AND METHODS

Cell lines and reagents

The A375P and A375MEA-3 cells lines were kindly provided by Lei Xu and Richard Hynes, Howard Hughes Medical Institute (HHMI) investigator at the Massachusetts Institute of Technology. All the other cell lines used in this study were acquired from the American Type Culture Collection (Manassas, VA). A375P, MIA-PaCa-2, HT1080, A375MEA-3, and MDA-MB-231 cells were cultured in DMEM supplemented with 10% (vol/vol) fetal bovine serum (FBS), 2 mM L-glutamine, 1 mM sodium pyruvate, and 1% (vol/vol) penicillin and streptomycin. BxPC-3 and AsPC-1 cell lines were cultured in RPMI media, supplemented as above. All the lines have been recently authenticated and tested for contamination. Antibodies used in this study include mouse anti-Hic-5, mouse anti-paxillin (clone349, Cat#610052; BD Biosciences, Franklin Lakes, NJ), rabbit anti-paxillin (H114, Cat#D1615), rabbit anti-GFP (Cat# sc-8334'; Santa Cruz, CA), rabbit anti-fibronectin (Cat#610077) and mouse anti-vinculin (Cat#V9131; Sigma Aldrich, St. Louis, MO), rabbit anti-FAK/PYK2 pTyr397 (Cat#700255; Invitrogen, Carlsbad, CA), and mouse immunoglobulin G1 (Cell Signaling Technologies, Danvers, MA; Deakin and Turner, 2011). Rhodamine-phalloidin, Acti-stain 670 (Cytoskeleton, Denver, CO), and 4'6-diamidine-2'-phenylindole (DAPI) (Sigma Aldrich, St. Louis, MO) were used to stain the F-actin cytoskeleton and nucleus, respectively. DyLight 488 and DyLight 633 conjugated anti-mouse and anti-rabbit antibodies (Thermo Fisher, Waltham, MA) were used for all immunofluorescence studies. Rac1 inhibitor NSC23766 (MilliporeSigma, Burlington, MA) was used at a concentration of 50 μM (Sanz-Moreno *et al.*, 2008).

Cell-derived matrix generation, 3D migration, and plasticity analyses

The 3D CDMs were generated using human foreskin fibroblasts as previously described (Deakin and Turner, 2011). For live cell analyses, cells were plated onto CDMs for 4 h and then tracked live using a Nikon TE2000 microscope equipped with an environmental chamber. Images were acquired at 10 min intervals for 16 h. The cell morphology index was quantified after 8 h from movies or fixed images, by measuring the cell circularity and Feret's diameter as described previously (Deakin and Turner, 2011). Plasticity was scored when a cell transitioned between a round and an elongated phenotype one or more times within the experimental time course. Cells undergoing mitosis were not included in the analyses.

Preparation of fibronectin-coated 1D substrates

Fibronectin-coated micropatterned lines were prepared via deep-ultraviolet illumination, as previously described (Tseng *et al.*, 2011).

Briefly, a chrome-plated quartz photomask (Microtronics, Newtown, PA) was cleaned using water and wiped with Rain-X to generate a hydrophobic surface. A polyacrylamide gel mixture was polymerized for 1 h between the photomask and a silanized coverslip at room temperature. Once the gel was polymerized, the photomask was placed in an UVO-Cleaner 342 (Jelight, Irvine, CA) and illuminated with ultraviolet light for 3 min. The coverslips with gel were gently removed from the photomask and inverted over a drop of 5 mg/ml 1-Thyly-3-(3-dimethylaminopropyl) carbodiimide HCl (EDC) (ThermoFisher, Waltham, MA) and 10 mg/ml *N*-hydroxysuccinimide (ThermoFisher, Waltham, MA) solution for 15 min, and then washed with HEPES buffer (pH 8.5) and incubated with 10 µg/ml fibronectin for 1 h. The gels were then washed extensively in phosphate-buffered saline (PBS) before cells were plated.

Transfections and RNAi-mediated protein depletion

MDA-MB-231 cells were transfected with RNAi for 72 h before indicated experiments using oligofectamine LTX (ThermoFisher, Waltham, MA) following the manufacturer's standard protocol. RNAi oligonculeotides were used at a concentration of 0.1 µM per transfection. The RNAi sequences used were as follows: paxillin-1, 5′-CCCUGACGAAAGAGAAGCCUA-3′ and 5′-UAGGCUUCUCUUUCGUCAGGG-3′; paxillin-2, 5′-GUGUGGAGCCUUCUUUGGU-3′ and 5′-ACCAAAGAAGGCUCCACAC-3′; Hic-5–1, 5′-GGAGCUGGAUAGACUGAUG-3′ and 5′-CAUCAGUCUAUCCAGCUCC-3′; Hic-5–2, 5′-GGACCAGUCUGAAGAUAAG-3′ and control, 5′-ACUCUAUCUGCACGCUGACUU-3′ and 5′-GUCAGCGUGCAGAUAGAG UUU-3′ (Deakin and Turner, 2011).

MDA-MB-231 and A375MEA-3 cells were transfected with GFP and YFP-tagged constructs using lipofectamine LTX (ThermoFisher, Waltham, MA), whereas the AsPC-1 and A375P cells were transfected using lipofectamine 3000 (ThermoFisher, Waltham, MA), following the manufacturer's standard protocol as indicated. Cells were spread on 2D fibronectin coverslips, into 3D CDMs, or fibronectin-coated micropatterned lines 24 h posttransfection. Quantitation of the mean fluorescence intensities of total vinculin, performed by staining with the anti-vinculin antibody in cells expressing YFP only or YFP-vinculin WT, T12, or A50I mutants indicate that the transfected constructs are expressed at approximately twofold excess over endogenous vinculin (unpublished data).

Immunofluorescence microscopy

Glass coverslips were coated with10 µg/ml fibronectin in PBS for 1 h at room temperature. Cells were fixed using 4% (wt/vol) paraformaldehyde in PBS for 15 min at room temperature. Cells were then permeabilized with 1% (vol/vol) Triton X-100 in PBS for 5 min at room temperature. Coverslips were washed three times with PBS and quenched with 0.1 M glycine for 15 min. Coverslips were then blocked with 3% (wt/vol) bovine serum albumin (BSA) for 16 h at 4°C. Samples were then incubated with primary antibodies, diluted in 3% BSA (1:100) in PBS as indicated, for 2 h at 37°C in a humidified chamber. Coverslips were then washed with PBS containing 0.05% (vol/vol) Tween-20 (PBST). Coverslips were incubated with appropriate Dylight-conjugated secondary antibodies and rhodamine-phalloidin diluted in PBST for 45 min at room temperature. Cells were washed twice and then stained with DAPI before being mounted on slides. Samples were imaged using a Leica SP5 laser scanning confocal microscope and a HPX Plan Apochromat 63×/1.4 NA oil λ BL objective or a Zeiss Axioskop2 plus microscope, fitted with a Q imagin ExiBlue charge-coupled device camera using an Apochromat 63×/0.75 NA objective.

Invasion assays

An inverted collagen and fibronectin invasion plug invasion assay (Caswell *et al.*, 2007; Provenzano *et al.*, 2008; Rowe *et al.*, 2009) was performed as previously described (Deakin and Turner, 2011). Briefly, transwell inserts (Corning, Corning, NY) were coated with 1 µg/ml FN for 30 min at 37°C. Cells (10^5) were seeded and allowed to adhere for 1 h. Collagen I (PureCol; Advanced Biomatrix, San Diego, CA) was mixed with 10× MEM at a 5:1 ratio along with fibronectin at 25 µg/ml was allowed to polymerize in the transwell inserts (Corning, Corning, NY) for 1 h at 37°C in the absence of CO_2. DMEM with 10% FBS was added to the transwells and they were placed in 1 ml of serum-free media. The transwells were incubated for 24 h and then stained with Calcein AM (Life Technologies, Carlsbad,CA) and visualized by confocal microscopy. The Matrigel invasion assay was performed as previously described (Wormer *et al.*, 2012). Briefly, 15,000 cells were plated per well into the upper chamber of the Matrigel-coated transwell insert with 0.8 µm pores (BD Bioscience, Franklin Lakes, NJ). The bottom chamber contained 10% (vol/vol) FBS-containing DMEM. Cells were allowed to invade through the chamber for 12 h. The cells on the top of each chamber were scraped with a cotton swab. The chamber was then fixed with 4% paraformaldehyde and then mounted on a slide for quantitation of GFP-positive cells.

Proximity ligation assay

Proximity ligation assays were performed according to the manufacturer's instructions using the anti-mouse and anti-rabbit Duolink PLA probes as well as the Duolink PLA detection reagents (Sigma Aldrich, St. Louis, MO). Cells were stained with Acti-stain 670 and DAPI. The discrete PLA spots per cell were counted.

Statistical analysis

A one-way analysis of variance (ANOVA) with Dunnet's multiple comparison test was used to compare more than three sets of samples and a two-tailed unpaired Student's *t* test was applied to compare two samples. All data sets were acquired from at least three independent experiments. Data represent mean ± SEM of at least three independent experiments. *, $p < 0.05$, **, $p < 0.01$, and ***, $p < 0.001$.

ACKNOWLEDGMENTS

We thank the members of the Turner lab for insightful discussions. We thank Ian Forsythe for developing the constructs used in the work. We are grateful to Lei Xu and Richard Hynes, HHMI investigator at the Massachusetts Institute of Technology, for providing the A375MEA-3 cell line and to Christoph Ballestrem for providing the vinculin constructs. This work was supported by the National Institutes of Health (RO1 CA-163296 and GM-047607 to C.E.T.).

REFERENCES

Azuma K, Tanaka M, Uekita T, Inoue S, Yokota J, Ouchi Y, Sakai R (2005). Tyrosine phosphorylation of paxillin affects the metastatic potential of human osteosarcoma. Oncogene 24, 4754–4764.

Ballestrem C, Erez N, Kirchner J, Kam Z, Bershadsky A, Geiger B (2006). Molecular mapping of tyrosine-phosphorylated proteins in focal adhesions using fluorescence resonance energy transfer. J Cell Sci 119, 866–875.

Belletti B, Nicoloso MS, Schiappacassi M, Berton S, Lovat F, Wolf K, Canzonieri V, D'Andrea S, Zucchetto A, Friedl P, *et al.* (2008). Stathmin activity influences sarcoma cell shape, motility, and metastatic potential. Mol Biol Cell 19, 2003–2013.

Bellis SL, Miller JT, Turner CE (1995). Characterization of tyrosine phosphorylation of paxillin in vitro by focal adhesion kinase. J Biol Chem 270, 17437–17441.

Bhowmick NA, Neilson EG, Moses HL (2004). Stromal fibroblasts in cancer initiation and progression. Nature 432, 332–337.
Boyd NF, Martin LJ, Yaffe MJ, Minkin S (2011). Mammographic density and breast cancer risk: current understanding and future prospects. Breast Cancer Res 13, 223.
Brown MC, Turner CE (2004). Paxillin: adapting to change. Physiol Rev 84, 1315–1339.
Burridge K, Turner CE, Romer LH (1992). Tyrosine phosphorylation of paxillin and pp125FAK accompanies cell adhesion to extracellular matrix: a role in cytoskeletal assembly. J Cell Biol 119, 893–903.
Case LB, Baird MA, Shtengel G, Campbell SL, Hess HF, Davidson MW, Waterman CM (2015). Molecular mechanism of vinculin activation and nanoscale spatial organization in focal adhesions. Nat Cell Biol 17, 880–892.
Caswell PT, Spence HJ, Parsons M, White DP, Clark K, Cheng KW, Mills GB, Humphries MJ, Messent AJ, Anderson KI, *et al.* (2007). Rab25 associates with α5β1 integrin to promote invasive migration in 3D microenvironments. Dev Cell 13, 496–510.
Cohen DM, Kutscher B, Chen H, Murphy DB, Craig SW (2006). A conformational switch in vinculin drives formation and dynamics of a talin-vinculin complex at focal adhesions. J Biol Chem 281, 16006–16015.
Condeelis J, Segall JE (2003). Intravital imaging of cell movement in tumours. Nat Rev Cancer 3, 921–930.
Deakin NO, Ballestrem C, Turner CE (2012a). Paxillin and Hic-5 interaction with vinculin is differentially regulated by Rac1 and RhoA. PLoS One 7, e37990.
Deakin NO, Pignatelli J, Turner CE (2012b). Diverse roles for the paxillin family of proteins in cancer. Genes Cancer 3, 362–370.
Deakin NO, Turner CE (2008). Paxillin comes of age. J Cell Sci 121, 2435–2444.
Deakin NO, Turner CE (2011). Distinct roles for paxillin and Hic-5 in regulating breast cancer cell morphology, invasion, and metastasis. Mol Biol Cell 22, 327–341.
Demali KA, Barlow CA, Burridge K (2002). Recruitment of the Arp2/3 complex to vinculin: coupling membrane protrusion to matrix adhesion. J Cell Biol 159, 881–891.
Derynck R, Akhurst RJ, Balmain A (2001). TGF-β signaling in tumor suppression and cancer progression. Nat Genet 29, 117–129.
Doyle AD, Wang FW, Matsumoto K, Yamada KM (2009). One-dimensional topography underlies three-dimensional fibrillar cell migration. J Cell Biol 184, 481–490.
Dumbauld DW, Lee TT, Singh A, Scrimgeour J, Gersbach CA, Zamir EA, Fu J, Chen CS, Curtis JE, Craig SW, Garcia AJ (2013). How vinculin regulates force transmission. Proc Natl Acad Sci USA 110, 9788–9793.
Eitaki M, Yamamori T, Meike S, Yasui H, Inanami O (2012). Vincristine enhances amoeboid-like motility via GEF-H1/RhoA/ROCK/Myosin light chain signaling in MKN45 cells. BMC Cancer 12, 469.
Friedl P, Alexander S (2011). Cancer invasion and the microenvironment: plasticity and reciprocity. Cell 147, 992–1009.
Friedl P, Wolf K (2003). Tumour-cell invasion and migration: diversity and escape mechanisms. Nat Rev Cancer 3, 362–374.
Friedl P, Wolf K (2010). Plasticity of cell migration: a multiscale tuning model. J Cell Biol 188, 11–19.
Gadea G, Sanz-Moreno V, Self A, Godi A, Marshall CJ (2008). DOCK10-mediated Cdc42 activation is necessary for amoeboid invasion of melanoma cells. Curr Biol 18, 1456–1465.
Goreczny GJ, Forsythe IJ, Turner CE (2018). Hic-5 regulates fibrillar adhesion formation to control tumor extracellular matrix remodeling through interaction with tensin1. Oncogene 37, 1699–1713.
Goreczny GJ, Ouderkirk-Pecone JL, Olson EC, Krendel M, Turner CE (2016). Hic-5 remodeling of the stromal matrix promotes breast tumor progression. Oncogene 36, 2693–2703.
Hetey SE, Lalonde DP, Turner CE (2005). Tyrosine-phosphorylated Hic-5 inhibits epidermal growth factor-induced lamellipodia formation. Exp Cell Res 311, 147–156.
Hildebrand JD, Schaller MD, Parsons JT (1995). Paxillin, a tyrosine phosphorylated focal adhesion-associated protein binds to the carboxyl terminal domain of focal adhesion kinase. Mol Biol Cell 6, 637–647.
Humphries JD, Wang P, Streuli C, Geiger B, Humphries MJ, Ballestrem C (2007). Vinculin controls focal adhesion formation by direct interactions with talin and actin. J Cell Biol 179, 1043–1057.
Mackinnon AC, Tretiakova M, Henderson L, Mehta RG, Yan BC, Joseph L, Krausz T, Husain AN, Reid ME, Salgia R (2011). Paxillin expression and amplification in early lung lesions of high-risk patients, lung adenocarcinoma and metastatic disease. J Clin Pathol 64, 16–24.
Mestayer C, Blanchere M, Jaubert F, Dufour B, Mowszowicz I (2003). Expression of androgen receptor coactivators in normal and cancer prostate tissues and cultured cell lines. Prostate 56, 192–200.
Nishi T, Takahashi H, Hashimura M, Yoshida T, Ohta Y, Saegusa M (2015). FilGAP, a Rac-specific Rho GTPase-activating protein, is a novel prognostic factor for follicular lymphoma. Cancer Med 4, 808–818.
Pankova K, Rosel D, Novotny M, Brabek J (2010). The molecular mechanisms of transition between mesenchymal and amoeboid invasiveness in tumor cells. Cell Mol Life Sci 67, 63–71.
Pignatelli J, Tumbarello DA, Schmidt RP, Turner CE (2012). Hic-5 promotes invadopodia formation and invasion during TGF-β–induced epithelial–mesenchymal transition. J Cell Biol 197, 421–437.
Provenzano PP, Inman DR, Eliceiri KW, Trier SM, Keely PJ (2008). Contact guidance mediated three-dimensional cell migration is regulated by Rho/ROCK-dependent matrix reorganization. Biophys J 95, 5374–5384.
Rahman A, Carey SP, Kraning-Rush CM, Goldblatt ZE, Bordeleau F, Lampi MC, Lin DY, Garcia AJ, Reinhart-King CA (2016). Vinculin regulates directionality and cell polarity in two- and three-dimensional matrix and three-dimensional microtrack migration. Mol Biol Cell 27, 1431–1441.
Rintoul RC, Sethi T (2002). Extracellular matrix regulation of drug resistance in small-cell lung cancer. Clin Sci (Lond) 102, 417–424.
Rowe RG, Li XY, Hu Y, Saunders TL, Virtanen I, Garcia de Herreros A, Becker KF, Ingvarsen S, Engelholm LH, Bommer GT, *et al.* (2009). Mesenchymal cells reactivate Snail1 expression to drive three-dimensional invasion programs. J Cell Biol 184, 399–408.
Sahai E, Marshall CJ (2003). Differing modes of tumour cell invasion have distinct requirements for Rho/ROCK signalling and extracellular proteolysis. Nat Cell Biol 5, 711–719.
Sanz-Moreno V, Gadea G, Ahn J, Paterson H, Marra P, Pinner S, Sahai E, Marshall CJ (2008). Rac activation and inactivation control plasticity of tumor cell movement. Cell 135, 510–523.
Sanz-Moreno V, Marshall CJ (2009). Rho-GTPase signaling drives melanoma cell plasticity. Cell Cycle 8, 1484–1487.
Sjogren U, Garwicz S (1980). Prognostic significance of amoeboid movement configuration in lymphoid cells from children with acute lymphoblastic leukaemia. Scand J Haematol 24, 335–339.
Sjogren U, Norberg B, Rydgren L (1977). Amoeboid movement configuration in tumour cells of bone marrow smears from patients with leukaemia. Incidence and significance. Acta Med Scand 201, 381–386.
Thievessen I, Fakhri N, Steinwachs J, Kraus V, Mcisaac RS, Gao L, Chen BC, Baird MA, Davidson MW, Betzig E, *et al.* (2015). Vinculin is required for cell polarization, migration, and extracellular matrix remodeling in 3D collagen. FASEB J 29, 4555–4567.
Thomas SM, Hagel M, Turner CE (1999). Characterization of a focal adhesion protein, Hic-5, that shares extensive homology with paxillin. J Cell Sci 112(Pt 2), 181–190.
Tseng Q, Wang I, Duchemin-Pelletier E, Azioune A, Carpi N, Gao J, Filhol O, Piel M, Thery M, Balland M (2011). A new micropatterning method of soft substrates reveals that different tumorigenic signals can promote or reduce cell contraction levels. Lab Chip 11, 2231–2240.
Tumbarello DA, Brown MC, Hetey SE, Turner CE (2005). Regulation of paxillin family members during epithelial-mesenchymal transformation: a putative role for paxillin delta. J Cell Sci 118, 4849–4863.
Tumbarello DA, Brown MC, Turner CE (2002). The paxillin LD motifs. FEBS Lett 513, 114–118.
Tumbarello DA, Turner CE (2007). Hic-5 contributes to epithelial-mesenchymal transformation through a RhoA/ROCK-dependent pathway. J Cell Physiol 211, 736–747.
Turner CE, Brown MC, Perrotta JA, Riedy MC, Nikolopoulos SN, Mcdonald AR, Bagrodia S, Thomas S, Leventhal PS (1999). Paxillin LD4 motif binds PAK and PIX through a novel 95-kD ankyrin repeat, ARF-GAP protein: A role in cytoskeletal remodeling. J Cell Biol 145, 851–863.
Turner CE, Glenney JR, Burridge K (1990). Paxillin: a new vinculin-binding protein present in focal adhesions. J Cell Biol 111, 1059–1068.
Wolf K, Friedl P (2006). Molecular mechanisms of cancer cell invasion and plasticity. Br J Dermatol 154(Suppl 1), 11–15.
Wolf K, Mazo I, Leung H, Engelke K, Von Andrian UH, Deryugina EI, Strongin AY, Brocker EB, Friedl P (2003a). Compensation mechanism in tumor cell migration: mesenchymal-amoeboid transition after blocking of pericellular proteolysis. J Cell Biol 160, 267–277.
Wolf K, Muller R, Borgmann S, Brocker EB, Friedl P (2003b). Amoeboid shape change and contact guidance: T-lymphocyte crawling through fibrillar collagen is independent of matrix remodeling by MMPs and other proteases. Blood 102, 3262–3269.

Wormer D, Deakin NO, Turner CE (2012). CdGAP regulates cell migration and adhesion dynamics in two- and three-dimensional matrix environments. Cytoskeleton (Hoboken) 69, 644–658.
Xu L, Shen SS, Hoshida Y, Subramanian A, Ross K, Brunet JP, Wagner SN, Ramaswamy S, Mesirov JP, Hynes RO (2008). Gene expression changes in an animal melanoma model correlate with aggressiveness of human melanoma metastases. Mol Cancer Res 6, 760–769.
Yamazaki D, Kurisu S, Takenawa T (2009). Involvement of Rac and Rho signaling in cancer cell motility in 3D substrates. Oncogene 28, 1570–1583.
Yeung KT, Yang J (2017). Epithelial-mesenchymal transition in tumor metastasis. Mol Oncol 11, 28–39.
Yu JA, Deakin NO, Turner CE (2010). Emerging role of paxillin-PKL in regulation of cell adhesion, polarity and migration. Cell Adh Migr 4, 342–347.
Zaidel-Bar R, Ballestrem C, Kam Z, Geiger B (2003). Early molecular events in the assembly of matrix adhesions at the leading edge of migrating cells. J Cell Sci 116, 4605–4613.
Zaidel-Bar R, Milo R, Kam Z, Geiger B (2007). A paxillin tyrosine phosphorylation switch regulates the assembly and form of cell-matrix adhesions. J Cell Sci 120, 137–148.